

# Dielectric Profiles and Ion-Specific Effects at Aqueous Interfaces

Douwe Jan Bonthuis<sup>1</sup> & Roland R. Netz<sup>2</sup>

<sup>1</sup>Rudolf Peierls Centre for Theoretical Physics, University of Oxford, Oxford OX1 3NP, United Kingdom

<sup>2</sup>Fachbereich Physik, Freie Universität Berlin, 14195 Berlin, Germany

## Contents

<b>1</b>	<b>Introduction</b>	<b>1</b>
<b>2</b>	<b>Calculation of the dielectric profile</b>	<b>1</b>
2.1	Construction of the dielectric dividing surface	3
<b>3</b>	<b>The modified Poisson-Boltzmann equation</b>	<b>3</b>
3.1	Double-layer capacitance	3
<b>4</b>	<b>Ion-specific effects</b>	<b>4</b>
<b>5</b>	<b>Summary and conclusions</b>	<b>5</b>

## 1 Introduction

Unlike bulk water, water at aqueous interfaces exhibits a pronounced anisotropic molecular ordering. The water density shows a depletion in the interfacial region, to an extent depending on ambient pressure and temperature [1] and on the hydrophobicity of the surface [2]. Moreover, at soft surfaces, such as air-water interfaces, the density increases monotonically, whereas at most solid surfaces the water molecules arrange in distinct layers, leading to an oscillating density profile [3]. Finally, vibrational spectroscopy experiments show that the water molecules in the interfacial region are preferentially oriented with their dipole moments pointing roughly along the surface plane at both air-water interfaces [4] and quartz-water interfaces [5, 6]. For macroscopic solutes, this molecular structure strongly affects both their static properties, such as double-layer capacitance and surface conductance, and their dynamic behavior, such as electro-osmotic mobility.

In this chapter, we present a modeling approach where we calculate the molecular properties, in particular the dielectric profile, from molecular dynamics (MD) simulations and incorporate the results into a modified Poisson-Boltzmann equation. Our MD simulations show that the aqueous interface can be characterized by two largely independent characteristic length scales: the dielectric dividing surface, based on the dielectric profile, and the Gibbs dividing surface, based on the water density profile. Using these two interface characteristics, we estimate two of the main contributions to the interaction between a surface and a single ion.

## 2 Calculation of the dielectric profile

If the electric field is independent of the spatial coordinates  $\mathbf{r}$ ,  $\mathbf{E}(\mathbf{r}) = \mathbf{E}$ , a change in the global electric field  $\Delta\mathbf{E}$  is related to a change in the local displacement field  $\Delta\mathbf{D}(\mathbf{r})$  by the tensorial local response function  $\varepsilon(\mathbf{r})$ ,

$$\Delta\mathbf{D}(\mathbf{r}) = \varepsilon_0\varepsilon(\mathbf{r}) \cdot \Delta\mathbf{E}, \quad (1)$$

with  $\varepsilon_0$  being the permittivity of vacuum and  $\varepsilon(\mathbf{r})$  being the integral over one argument of the nonlocal dielectric response function [7]. Similarly, a change in the homogeneous displacement field,  $\Delta\mathbf{D}$ , is related to a change in the local electric field  $\Delta\mathbf{E}(\mathbf{r})$  by the inverse dielectric response function  $\varepsilon^{-1}(\mathbf{r})$ ,

$$\Delta\mathbf{E}(\mathbf{r}) = \varepsilon_0^{-1}\varepsilon^{-1}(\mathbf{r}) \cdot \Delta\mathbf{D}, \quad (2)$$

with  $\varepsilon^{-1}(\mathbf{r})$  the inverse dielectric function. To calculate the dielectric function from the polarization of the medium, the electric field  $\mathbf{E}(\mathbf{r})$  is separated into the displacement field  $\mathbf{D}(\mathbf{r})$ , associated with the monopole density  $P_0(\mathbf{r})$ , and the polarization  $\mathbf{m}(\mathbf{r})$ , generated by all higher order multipole moments,  $\varepsilon_0\mathbf{E}(\mathbf{r}) = \mathbf{D}(\mathbf{r}) - \mathbf{m}(\mathbf{r})$ . We consider water at a planar surface, having translational invariance in the  $x$  and  $y$  directions and a dielectric discontinuity in the  $z$  direction. In this planar geometry, the dielectric tensor is diagonal with only two unique components, one parallel and one perpendicular to the surface, and the electric field and the polarization density depend on the  $z$  direction only. Maxwell's equation  $\nabla \times \mathbf{E}(z) = 0$  implies that  $E_{\parallel}$ , corresponding to  $E_x$

or  $E_y$ , is independent of  $z$  everywhere. With the symmetry condition  $\Delta E_{\parallel} = E_{\parallel}$ , the parallel component of Eq. 1 becomes

$$\varepsilon_{\parallel}(z) = 1 + \frac{\Delta m_{\parallel}(z)}{\varepsilon_0 E_{\parallel}}. \quad (3)$$

When the monopole density  $P_0(z) = 0$ , Maxwell's equation for the displacement field,  $\nabla \cdot \mathbf{D}(z) = P_0(z)$ , shows that the displacement field is constant in space. Using the boundary condition  $\Delta D_{\perp}(z) = D_{\perp}$ , the perpendicular component of the inverse dielectric function given in Eq. 2 becomes

$$\varepsilon_{\perp}^{-1}(z) = 1 - \frac{\Delta m_{\perp}(z)}{D_{\perp}}. \quad (4)$$

Applying an external electric field, the dielectric tensor can be calculated directly from Eqs. 3 and 4. To estimate the dielectric response from the fluctuations of the polarization in absence of an external field, we use a statistical mechanical expression for the excess polarization  $\Delta \mathbf{m}(\mathbf{r})$  upon application of an external field. For small applied field  $\mathbf{F}$ , the linearized ensemble average of the excess polarization vector is given by [8, 9, 10]

$$\Delta \mathbf{m}(\mathbf{r}) \approx \beta [\langle \mathbf{m}(\mathbf{r}) \mathbf{M} \rangle_0 - \langle \mathbf{m}(\mathbf{r}) \rangle_0 \langle \mathbf{M} \rangle_0] \cdot \mathbf{F}, \quad (5)$$

where  $\langle \dots \rangle_0$  denotes the ensemble average without applied electric field. In order to determine the dielectric tensor, we need to know the relation between the applied field  $\mathbf{F}$  in Eq. 5 and  $\Delta \mathbf{E}$  or  $\Delta \mathbf{D}$  in Eqs. 1 and 2. In the direction parallel to the surface, the homogeneous applied field  $F_{\parallel}$  in Eq. 5 must correspond to the homogeneous field  $E_{\parallel}$ . Therefore, combining Eqs. 3 and 5 leads to

$$\varepsilon_{\parallel}(z) \approx 1 + \varepsilon_0^{-1} \beta [\langle m_{\parallel}(z) M_{\parallel} \rangle_0 - \langle m_{\parallel}(z) \rangle_0 \langle M_{\parallel} \rangle_0]. \quad (6)$$

In the direction perpendicular to the surface, the spatially constant field  $F_{\perp}$  must be associated with the homogeneous displacement field  $D_{\perp}/\varepsilon_0$ . Consequently, combining Eqs. 4 and 5, we arrive at the fluctuation equation for the inverse perpendicular permittivity,

$$\varepsilon_{\perp}^{-1}(z) \approx 1 - \varepsilon_0^{-1} \beta [\langle m_{\perp}(z) M_{\perp} \rangle_0 - \langle m_{\perp}(z) \rangle_0 \langle M_{\perp} \rangle_0]. \quad (7)$$

The polarization  $\mathbf{m}(\mathbf{r})$  can be calculated in two different ways. The first method is to express  $\mathbf{m}(\mathbf{r})$  in terms of the multipole densities [11, 7]

$$\mathbf{m}(\mathbf{r}) = \mathbf{P}_1(\mathbf{r}) - \nabla \cdot \mathbf{P}_2(\mathbf{r}) + \nabla \nabla : \mathbf{P}_3(\mathbf{r}) - \dots \quad (8)$$

The terms written explicitly are the dipole density  $\mathbf{P}_1$ , the quadrupole density  $\mathbf{P}_2$  and the octupole density  $\mathbf{P}_3$ . When each molecule  $i$  is composed of atoms  $j$  with point charges  $q_j^i$  at positions  $\mathbf{r}_j^i$ , the terms of Eq. 8 are set by the spatial distribution of partial charges,

$$P_l(\mathbf{r}) = \sum_i \mathbf{p}_{li} \delta(\mathbf{r} - \mathbf{r}_i) \quad \text{with} \quad \mathbf{p}_{li} = \frac{1}{l!} \sum_{j(i)} q_j^i (\mathbf{r}_j^i - \mathbf{r}_i)^l, \quad (9)$$

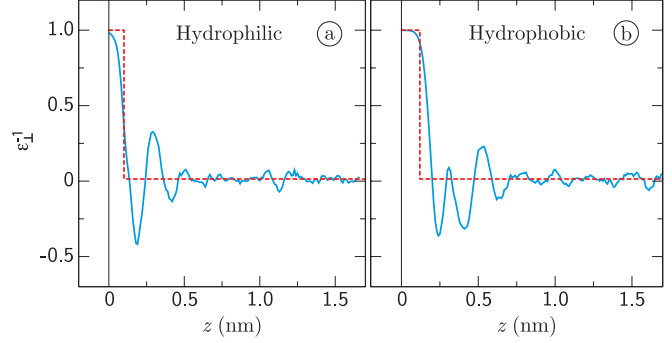


Figure 1: The inverse perpendicular dielectric profile (blue solid lines), calculated using Eqs. 7 and 10, for SPC/E water at (a) a hydrophilic (hydroxide-terminated) and (b) a hydrophobic (hydrogen-terminated) diamond surface. See [7] for details of the MD simulations. Also shown is the step-function approximation of Eq. 12 (red dashed lines).

where  $\mathbf{p}_{li}$  denotes the molecular multipole moment of order  $l \in \{0, 1, 2, \dots\}$ , and  $\mathbf{r}_i$  is some reference point in the molecule. Alternatively, the perpendicular polarization density in absence of free charges,  $P_0(z) = 0$ , is calculated from an integral over the total charge density  $\rho(z) = \sum_{i,j} q_j^i \delta(\mathbf{r} - \mathbf{r}_j^i)$ ,

$$m_{\perp}(z) = - \int_0^z \rho(z') dz'. \quad (10)$$

To calculate the polarization  $m_{\parallel}$  in the direction parallel to the surface, we introduce a virtual cut perpendicular to the  $x$  axis, where the  $x$  direction can be any direction parallel to the surface. We only cut the water molecules at the position of the virtual cut, closing the volume without cutting any other molecules. By cutting the volume, some water molecules are split, forming a non-zero monopole density  $P_0(x, z)$  on either side of the virtual cut, where the  $x$  dependence of  $P_0(x, z)$  has the form of a Dirac delta function at the position of the cut. For more details, see [7]. The parallel polarization density is calculated from

$$m_{\parallel}(z) = \pm \int P_0(x, z) dx, \quad (11)$$

where the different signs apply to closing the volume and integrating  $P_0(x, z)$  on the different sides of the cut. To calculate  $m_{\parallel}(z)$ , Eq. 11 is averaged over many different cut positions along the  $x$  axis.

The dielectric profiles calculated from either the fluctuations or the response to an applied field, and using either of the methods described above to calculate  $\mathbf{m}(\mathbf{r})$ , all coincide [7]. Interestingly,  $\varepsilon_{\perp}^{-1}(z)$  shows strong oscillations – even passing through zero several times – within the first few water layers, reflecting the molecular structure at the interface (Fig. 1).

## 2.1 Construction of the dielectric dividing surface

For further investigation of the effect of the dielectric profile on macroscopic interfacial properties, such as the double-layer capacitance, the electrophoretic mobility and the surface conductivity, it is convenient to simplify the dielectric profile. We approximate the profile shown in Fig. 1 with a step function,

$$\varepsilon_{\perp}(z) = \begin{cases} 1 & \text{if } z < z_{\perp}^{\text{DDS}} \\ \varepsilon_{\text{bulk}} & \text{otherwise.} \end{cases} \quad (12)$$

The dielectric dividing surface position in Eq. 12 is defined as

$$z_{\perp}^{\text{DDS}} = z_v + \int_{z_v}^{z_l} \frac{\varepsilon_{\perp}^{-1}(z_l) - \varepsilon_{\perp}^{-1}(z)}{\varepsilon_{\perp}^{-1}(z_l) - \varepsilon_{\perp}^{-1}(z_v)} dz, \quad (13)$$

with  $z_v$  and  $z_l$  being positions in the solid and liquid phase, respectively. The profile in Eq. 12 is designed to reproduce the electrostatic potential calculated in molecular dynamics simulations at positions  $z \gtrsim 1$  nm from the interface [12]. The definition of the dielectric dividing surface in Eq. 13 is analogous to the definition of the Gibbs dividing surface, which follows from Eq. 13 by replacing the dielectric profile  $\varepsilon_{\perp}^{-1}(z)$  by the water density profile. On a simple level, the effects of the dielectric profile and the density profile can be quantified using these two length scales. For  $z_{\perp}^{\text{DDS}}$  we use two different values:  $z_{\perp}^{\text{DDS}} = 0.10$  nm, corresponding to a hydrophilic surface, and  $z_{\perp}^{\text{DDS}} = 0.12$  nm, corresponding to a very hydrophobic surface [7]. With its insensitivity to surface type,  $z_{\perp}^{\text{DDS}}$  stands in strong contrast to the Gibbs dividing surface  $z^{\text{GDS}}$ , which lies much closer to the surface at hydrophilic surfaces ( $z^{\text{GDS}} = 0.07$  nm) than at hydrophobic surfaces ( $z^{\text{GDS}} = 0.22$  nm). The inverse dielectric profiles  $\varepsilon_{\perp}^{-1}(z)$  in the step-function approximation of Eq. 12 are shown as red dashed lines in Fig. 1.

## 3 The modified Poisson-Boltzmann equation

At charged surfaces, the monopole density  $P_0(z)$  is non-zero, and consequently the displacement field  $D_{\perp}(z)$  is not homogeneous. Therefore, we use the local assumption that the electric field  $E_{\perp}(z)$  is linearly related to  $D_{\perp}(z)$  by  $\varepsilon_{\perp}^{-1}(z)$ ,

$$\varepsilon_0 E_{\perp}(z) = \varepsilon_{\perp}^{-1}(z) D_{\perp}(z). \quad (14)$$

Eq. 14 is a good approximation in case of a slowly varying  $D_{\perp}(z)$  [12, 13]. Taking the derivative of Eq. 14 and using  $\nabla\psi(z) = -E_{\perp}(z)$ , with  $\psi(z)$  the electrostatic potential, and  $\nabla D_{\perp}(z) = P_0(z)$ , with  $P_0(z)$  the ionic charge density, the Poisson equation is transformed into an integro-differential equation,

$$\varepsilon_0 \nabla^2 \psi(z) = -\varepsilon_{\perp}^{-1}(z) P_0(z) - D_{\perp}(z) \nabla \varepsilon_{\perp}^{-1}(z), \quad (15)$$

with the displacement field  $D_{\perp}(z)$  being given by

$$D_{\perp}(z) = \int_0^z P_0(z') dz'. \quad (16)$$

Considering a solution of monovalent ions, the free charge density is calculated from the ionic densities  $c_+(z)$  and  $c_-(z)$ ,

$$P_0(z) = e(c_+(z) - c_-(z)), \quad (17)$$

with  $e$  the absolute charge of an electron. To ensure that the ionic density does not exceed its physical limit set by the ionic volume, we include a fermionic steric interaction to calculate the ionic densities from the unrestricted ionic densities  $\tilde{c}_+(z)$  and  $\tilde{c}_-(z)$  [14, 15, 16, 17, 18],

$$c_{\pm}(z) = \frac{\sqrt{2} \tilde{c}_{\pm}(z)}{\sqrt{2} + a_{\pm}^3 (\tilde{c}_{\pm}(z) - c_0) + a_{\mp}^3 (\tilde{c}_{\mp}(z) - c_0)}, \quad (18)$$

with  $c_0$  the bulk salt concentration and  $a_+$  and  $a_-$  the diameters of positive and negative ions, respectively. The denominator in Eq. 18 restricts the maximum density  $c_{\pm}(z)$  to  $\sqrt{2} a_{\pm}^{-3}$ , which is the maximum density of close-packed (face-centered cubic or hexagonal close-packed) spheres of diameter  $a_{\pm}$ . The unrestricted ionic densities  $\tilde{c}_+(z)$  and  $\tilde{c}_-(z)$  follow the Boltzmann distribution

$$\tilde{c}_{\pm}(z) = c_0 \exp[-\mu_{\pm}(z) \mp \beta e \psi(z)], \quad (19)$$

with  $\beta$  being the inverse thermal energy and  $\mu_+(z)$  and  $\mu_-(z)$  being the non-electrostatic contributions to the potentials of the positive and negative ions, respectively. Combining Eqs. 15-19 yields the modified Poisson-Boltzmann equation. It should be noted that the steric interaction of Eq. 18 becomes important only in case of high surface charge density, high salt concentration or large ion size [19]; its effect on the calculations presented here is minor.

For the non-electrostatic potential  $\mu_{\pm}(z)$ , we use a heuristic function of the form

$$\mu_{\pm}(z) = \alpha \exp[1 - 2z/a_{\pm}]. \quad (20)$$

Beyond 1 nm away from the interface, the potential of mean force – which includes dielectric as well as non-electrostatic effects – typically shows a decreasing shape that can be well approximated with the exponential form of Eq. 20 [20, 21].

### 3.1 Double-layer capacitance

To demonstrate the experimentally relevant consequences of the dielectric profile determined in Section 3, we calculate the double-layer capacitance and compare the result to experimental data. We solve Eqs. 15-19 at a surface with surface charge density  $\sigma_0$ , using the boundary conditions  $\lim_{z \rightarrow \infty} \psi(z) = 0$  and overall charge neutrality. The capacitance  $C$  is calculated in the limit  $\sigma_0 \rightarrow 0$  from  $C = d\sigma_0/d\psi_0$ , with  $\psi_0$  the potential at

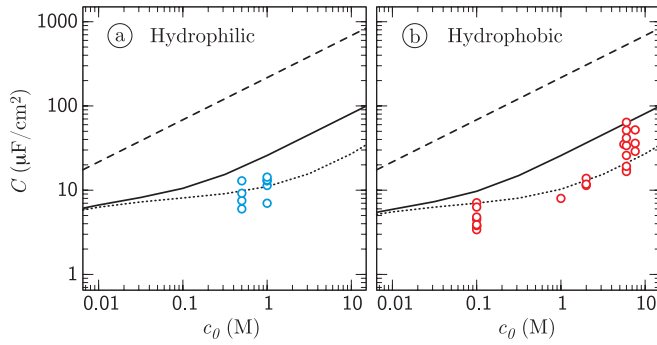


Figure 2: Double-layer capacitance  $C$  as a function of the bulk salt concentration  $c_0$ . Symbols represent experimental results on different kinds of (a) hydrophilic and (b) hydrophobic carbon-based surfaces [12]. Curves represent theoretical results using  $\varepsilon_{\perp}(z) = \varepsilon_{bulk}$  with  $\mu_{\pm}(z) = 0$  (dashed lines),  $\varepsilon_{\perp}(z)$  from Eq. 12 with  $\mu_{\pm}(z) = 0$  (solid lines), and  $\varepsilon_{\perp}(z)$  from Eq. 12 with  $\mu_{\pm}(z)$  from Eq. 20 using  $\alpha = 1$  (dotted lines). The ionic diameter  $a_{\pm} = 0.3$  nm for all curves.

$z = 0$ . Assuming  $\varepsilon_{\perp}(z) = \varepsilon_{bulk}$  (dashed lines in Fig. 2), the result of the Poisson-Boltzmann equation overestimates the experimental data by one order of magnitude. Better agreement with the experimental data is obtained when the dielectric profile is taken into account via Eq. 12 (solid lines in Fig. 2), which effectively introduces an interfacial layer with a low dielectric constant, much alike the Stern layer [22]. The experimental results can be fitted quantitatively using the non-electrostatic potential  $\mu_{\pm}(z)$  of Eq. 20 in addition to the dielectric profile (dotted lines in Fig. 2), where the interaction strength  $\alpha$  is used as a fitting parameter to account for the data spread due to the different surface materials and ion types used in the experiments. The interaction strength needed to fit the data is of order unity; for the dotted curves in Fig. 2 we have used  $\alpha = 1$ . Interestingly, the experimental data demonstrate that the hydrophobicity of the surface has no significant influence on the double-layer capacitance, which can be viewed as a confirmation of our result that the values of  $z_{\perp}^{DDS}$  hardly differ between the two surface types.

Using the modeling approach presented in Secs. 2 and 3 in conjunction with a modified Navier Stokes equation, we have also been able to theoretically model electrokinetic measurements, in particular the electrophoretic mobility and the so-called anomalous surface conductivity [23].

## 4 Ion-specific effects

In the calculations expounded in Section 3, the potential energy of an ion consists of the electrostatic energy of a point charge in the mean electrostatic potential, and a non-electrostatic term for which the simplified form of Eq. 20 is used. Experimentally, however, the energy of interaction between an ion and a surface is found to

depend on the ion's chemical properties, such as size, charge and polarizability, and is strongly ion-specific [24]. Models of the specific ion-surface interaction have been developed based on polarizability and hydration effects [25, 26]. Equally important for the ion-specific interaction are the molecular structure of the interfacial water and the chemical properties of the surface [21]. The combined potential due to the aforementioned effects is termed the potential of mean force (PMF), which can be incorporated into the Poisson-Boltzmann equation as a non-electrostatic contribution to the potential. Previous attempts, however, to split the PMF into contributions from the Lennard-Jones potential, the polarizability, the image charge potential and the electrostatics of the ordered water molecules, have failed to capture the results from atomistic MD simulations [20].

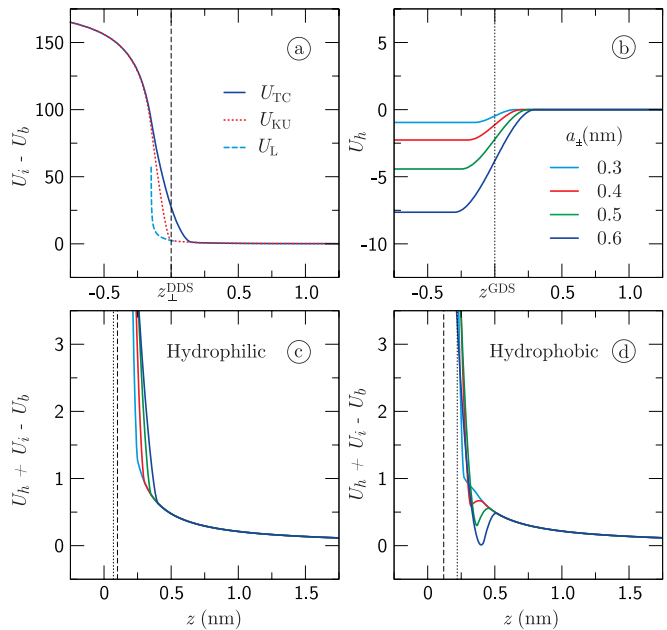


Figure 3: (a) Image charge potential  $U_i(z) - U_b$  of a non-polarizable ( $U_{TC}(z)$  [27]) and a perfectly polarizable ( $U_L(z)$  [25]) ion of diameter  $d_{\pm} = 0.3$  nm in the dielectric profile of Eq. 12. Also shown is the flawed Kharkats & Ulstrup potential  $U_{KV}(z)$  [28, 29]. (b) Hydration potential  $U_h(z)$  (Eq. 22) and the sum  $U_h(z) + U_i(z) - U_b$  at (c) hydrophilic and (d) hydrophobic surfaces, using  $U_i(z) = U_{TC}(z)$ , for ions of different diameter  $a_{\pm} = d_{\pm}$  (legend as in b). Positions of the dielectric dividing surface (dashed vertical lines) and Gibbs dividing surface (dotted vertical lines) are also shown.

Based on the two length scales discussed above, the Gibbs dividing surface  $z_{\perp}^{GDS}$  and dielectric dividing surface  $z_{\perp}^{DDS}$ , we design a model for ion-surface interactions that combines the image charge potential, which does not appear in a proper mean-field formulation, and the non-electrostatic hydration energy. The model is aimed at capturing the main features of the ionic PMF. The image potential depends on the distance  $z'$  to the dielectric dividing surface position,  $z' = z - z_{\perp}^{DDS}$ , and on the

size of the ion. For the latter, we introduce the dielectric diameter  $d_{\pm}$  as a second ionic diameter next to the ionic hard-sphere diameter  $a_{\pm}$ . The dielectric diameter can be estimated by equating the experimental solvation free energy to the sum of the electrostatic energy and the cavity hydration energy. Because the cavity contribution to the solvation free energy can be neglected for small ions, the dielectric diameter can be approximated by equating the ionic solvation free energy to the electrostatic energy  $U_b(1 - \varepsilon_{bulk})$ , with  $U_b$  being the Born free energy, given by

$$U_b = \frac{\beta e^2}{4\pi d_{\pm} \varepsilon_0 \varepsilon_{bulk}}. \quad (21)$$

For small ions, we expect that  $d_{\pm} > a_{\pm}$ , reflecting the observation that diameters inferred from the solvation free energy are larger than cavity diameters measured with diffraction methods [30]. Given the hydrophilic nature of small ions, it also conforms with our result that  $z_{\perp}^{\text{DDS}} > z^{\text{GDS}}$  at hydrophilic surfaces. However, the relation between  $a_{\pm}$  and  $d_{\pm}$  may be different for larger ions. In the following calculations, we choose  $a_{\pm} = d_{\pm}$  for simplicity. The image potential  $U_i(z)$  with respect to the Born energy  $U_b$  is calculated numerically for a non-polarizable finite-sized ion with  $d_{\pm} = 0.3$  nm ( $U_{\text{TC}}(z)$  in Fig. 3a) [27]. Also shown in Fig. 3a are an approximate expression for a perfectly polarizable ion, denoted  $U_L(z)$  [25], and the flawed expression  $U_{\text{KV}}(z)$  [28, 29] used in previous studies [7], the latter of which lies in between the results for a perfectly polarizable and a non-polarizable ion. In order to compare to MD simulations with non-polarizable force fields, we use  $U_i(z) = U_{\text{TC}}(z)$  to calculate the total interaction energy.

In addition to the repulsive image potential, the ions are subject to an attractive hydration potential, scaling with the hydrated volume of the ion [31, 32, 33]. Calculating the ionic volume from the hard-sphere cavity diameter  $a_{\pm}$ , the hydration energy is given by

$$U_h(z) = \begin{cases} -\frac{\pi}{6} a_{\pm}^3 \beta C & \text{if } 2z'' < -a_{\pm} \\ 0 & \text{if } 2z'' > a_{\pm} \\ -\frac{\pi}{12} (a_{\pm} - 2z'')^2 (z'' + a_{\pm}) \beta C & \text{otherwise,} \end{cases} \quad (22)$$

with  $z'' = z - z^{\text{GDS}}$ ,  $\beta$  being the inverse thermal energy and  $C = 2.8 \times 10^{-19}$  J/nm<sup>3</sup> being the hydration energy of an uncharged cavity in bulk water [34]. Importantly,  $U_i(z)$  and  $U_h(z)$  act with respect to different surface positions: while the image potential acts with respect to  $z_{\perp}^{\text{DDS}}$  (Fig. 3a), the hydration potential of Eq. 22 acts with respect to  $z^{\text{GDS}}$  (Fig. 3b). A major difference between hydrophilic and hydrophobic surfaces is that whereas  $z^{\text{GDS}} < z_{\perp}^{\text{DDS}}$  at hydrophilic surfaces, their order is reversed at hydrophobic surfaces. Because  $z^{\text{GDS}} > z_{\perp}^{\text{DDS}}$  at hydrophobic surfaces, the influence of the attractive hydration potential is much more pronounced than it is at hydrophilic surfaces. The total interaction potential  $U_h(z) + U_i(z) - U_b$  clearly reflects this difference between

hydrophilic (Fig. 3c) and hydrophobic (Fig. 3d) surfaces: whereas big ions ( $d_{\pm} = 0.6$  nm, corresponding to iodide) are repelled from hydrophilic surfaces, they are adsorbed on to hydrophobic surfaces, similar to the results of recent MD simulations [21]. Small ions ( $d_{\pm} = 0.3$  nm, corresponding to fluoride and sodium) are repelled from both surface types.

## 5 Summary and conclusions

We have presented the theoretical framework to extract the dielectric profile of interfacial water from MD simulations. Incorporating the dielectric profile into a modified mean-field description of the interfacial electrostatics, we have shown that taking the dielectric properties of pure interfacial water into account is necessary to capture the experimental values of the double-layer capacitance. Characterizing the dielectric profile and the density profile of water with two independent length scales, namely the dielectric dividing surface and the Gibbs dividing surface, a simple calculation of the ion-surface interaction potential exhibits a conspicuous difference between hydrophilic and hydrophobic surfaces: large ions that are readily adsorbed on to hydrophobic surfaces are still repelled from hydrophilic ones.

## References

- [1] Mamatkulov, S. I., Khabibullaev, P. K. & Netz, R. R. Water at hydrophobic substrates: Curvature, pressure, and temperature effects. *Langmuir* **20**, 4756 (2004).
- [2] Sendner, C., Horinek, D., Bocquet, L. & Netz, R. R. Interfacial water at hydrophobic and hydrophilic surfaces: Slip, viscosity, and diffusion. *Langmuir* **25**, 10768 (2009).
- [3] Sedlmeier, F. *et al.* Water at polar and nonpolar solid walls. *Biointerphases* **3**, FC23 (2008).
- [4] Du, Q., Superfine, R., Freysz, E. & Shen, Y. R. Vibrational spectroscopy of water at the vapor water interface. *Phys. Rev. Lett.* **70**, 2313 (1993).
- [5] Du, Q., Freysz, E. & Shen, Y. R. Surface vibrational spectroscopic studies of hydrogen bonding and hydrophobicity. *Science* **264**, 826 (1994).
- [6] Du, Q., Freysz, E. & Shen, Y. R. Vibrational spectra of water molecules at quartz/water interfaces. *Phys. Rev. Lett.* **72**, 238 (1994).
- [7] Bonthuis, D. J., Gekle, S. & Netz, R. R. Profile of the static permittivity tensor of water at interfaces: Consequences for capacitance, hydration interaction and ion adsorption. *Langmuir* **28**, 7679 (2012).

- [8] Kirkwood, J. G. The dielectric polarization of polar liquids. *J. Chem. Phys.* **7**, 911 (1939).
- [9] Fröhlich, H. *Theory of Dielectrics* (Clarendon Press, Oxford, 1949).
- [10] Ballenegger, V. & Hansen, J. Dielectric permittivity profiles of confined polar fluids. *J. Chem. Phys.* **122**, 114711 (2005).
- [11] Jackson, J. D. *Classical Electrodynamics* (John Wiley & Sons, USA, 1998), third edn.
- [12] Bonthuis, D. J., Gekle, S. & Netz, R. R. Dielectric profile of interfacial water and its effect on double-layer capacitance. *Phys. Rev. Lett.* **107**, 166102 (2011).
- [13] Kornyshev, A. A., Schmickler, W. & Vorotyntsev, M. A. Nonlocal electrostatic approach to the problem of a double layer at a metal-electrolyte interface. *Phys. Rev. B* **25**, 5244 (1982).
- [14] Bikerman, J. J. Structure and capacity of electrical double layer. *Philos. Mag.* **33**, 384 (1942).
- [15] Eigen, M. & Wicke, E. The thermodynamics of electrolytes at higher concentration. *J. Phys. Chem.* **58**, 702 (1954).
- [16] Kralj-Iglič, V. & Iglič, A. Influence of finite size of ions on electrostatic properties of electric double layer. *Electrotechnical Review (Ljubljana, Slovenija)* **61**, 127 (1994).
- [17] Borukhov, I., Andelman, D. & Orland, H. Steric effects in electrolytes: A modified Poisson-Boltzmann equation. *Phys. Rev. Lett.* **79**, 00319007 (1997).
- [18] Borukhov, I., Andelman, D. & Orland, H. Adsorption of large ions from an electrolyte solution: A modified Poisson-Boltzmann equation. *Electrochim. Acta* **46**, 221 (2000).
- [19] Bazant, M. Z., Kilic, M. S., Storey, B. D. & Ajdari, A. Towards an understanding of induced-charge electrokinetics at large applied voltages in concentrated solutions. *Adv. Colloid Interface Sci.* **152**, 48 (2009).
- [20] Horinek, D. *et al.* Molecular hydrophobic attraction and ion-specific effects studied by molecular dynamics. *Langmuir* **24**, 1271 (2008).
- [21] Schwierz, N., Horinek, D. & Netz, R. R. Reversed anionic Hofmeister series: The interplay of surface charge and surface polarity. *Langmuir* **26**, 7370 (2010).
- [22] Stern, O. Zur Theorie der elektrolytischen Doppelschicht. *Z. Elektrochem.* **30**, 508 (1924).
- [23] Bonthuis, D. J. & Netz, R. R. Unraveling the combined effects of dielectric and viscosity profiles on surface capacitance, electro-osmotic mobility, and electric surface conductivity. *Langmuir* **28**, 16049 (2012).
- [24] Kunz, W. Specific ion effects in colloidal and biological systems. *Curr. Opin. Colloid Interface Sci.* **15**, 34 (2010).
- [25] Levin, Y. Polarizable ions at interfaces. *Phys. Rev. Lett.* **102**, 147803 (2009).
- [26] Dos Santos, A. P., Diehl, A. & Levin, Y. Surface tensions, surface potentials, and the hofmeister series of electrolyte solutions. *Langmuir* **26**, 10778 (2010).
- [27] Tamashiro, M. N. & Constantino, M. A. Ions at the water-vapor interface. *J. Phys. Chem. B* **114**, 3583 (2010).
- [28] Kharkats, Y. I. & Ulstrup, J. The electrostatic Gibbs energy of finite-size ions near a planar boundary between 2 dielectric media. *J. Electroanal. Chem.* **308**, 17 (1991).
- [29] Markin, V. S. & Volkov, A. G. Quantitative theory of surface tension and surface potential of aqueous solutions of electrolytes. *J. Phys. Chem. B* **106**, 11810 (2002).
- [30] Marcus, Y. Ionic radii in aqueous solutions. *Chem. Rev.* **88**, 1475 (1988).
- [31] Horinek, D. *et al.* Specific ion adsorption at the air/water interface: The role of hydrophobic solvation. *Chem. Phys. Lett.* **479**, 173 (2009).
- [32] Huang, D. M., Geissler, P. L. & Chandler, D. Scaling of hydrophobic solvation free energies. *J. Phys. Chem. B* **105**, 6704 (2001).
- [33] Hummer, G., Garde, S., García, A. E., Paulaiti, M. E. & Pratt, L. R. Hydrophobic effects on a molecular scale. *J. Phys. Chem. B* **102**, 10469 (1998).
- [34] Huang, D. M., Cottin-Bizonne, C., Ybert, C. & Bocquet, L. Aqueous electrolytes near hydrophobic surfaces: Dynamic effects of ion specificity and hydrodynamic slip. *Langmuir* **24**, 1442 (2008).